

Article

Total and Partial Shear Viscosity in Heavy-Ion Collisions at Energies of BES, FAIR and NICA

Maksym Teslyk ^{1,2,†}, Larisa Bravina ^{1,†} and Evgeny Zabrodin ^{1,3,*†} 

¹ Department of Physics, University of Oslo, PB 1048 Blindern, N-0316 Oslo, Norway; machur@ukr.net (M.T.); larissa.bravina@fys.uio.no (L.B.)

² Faculty of Physics, Taras Shevchenko National University of Kyiv, UA-03022 Kyiv, Ukraine

³ Skobeltsyn Institute of Nuclear Physics, Moscow State University, RU-119991 Moscow, Russia

* Correspondence: zabrodin@fys.uio.no

† These authors contributed equally to this work.

Abstract: We calculated the shear viscosity of hot and dense nuclear matter produced in a symmetric system of central gold–gold collisions at energies of BES RHIC, FAIR and NICA. For calculations of the collisions, the transport model UrQMD was employed. The shear viscosity was obtained within the Green–Kubo formalism. The hadron resonance gas model was used to determine temperature and chemical potentials of baryon charge and strangeness out of microscopic model calculations. In contrast to our previous works, we determined the partial viscosity of the main hadron species, such as nucleons, pions, kaons and Lambdas, via the nucleon–nucleon, pion–pion and so forth, correlators. A decrease in the beam energy from $E_{lab} = 40$ to 10 AGeV leads a to rise in baryon shear viscosity accompanied by a drop in the shear viscosity of mesons. The ratio of total shear viscosity to entropy density also decreases.

Keywords: relativistic heavy-ion collisions; transport models; HRG model; shear viscosity; η/s ratio



Citation: Teslyk, M.; Bravina, L.; Zabrodin, E. Total and Partial Shear Viscosity in Heavy-Ion Collisions at Energies of BES, FAIR and NICA. *Symmetry* **2022**, *14*, 634. <https://doi.org/10.3390/sym14040634>

Academic Editor: Armen Sedrakian

Received: 18 February 2022

Accepted: 20 March 2022

Published: 22 March 2022

Publisher's Note: MDPI stays neutral with regard to jurisdictional claims in published maps and institutional affiliations.



Copyright: © 2022 by the authors. Licensee MDPI, Basel, Switzerland. This article is an open access article distributed under the terms and conditions of the Creative Commons Attribution (CC BY) license (<https://creativecommons.org/licenses/by/4.0/>).

1. Introduction

The interest in this topic is due to several reasons. The theory of strong interactions, quantum chromodynamics (QCD), predicts the transition of nuclear matter to a new state, called quark–gluon plasma QGP, at extremely high density and temperature; see, e.g., [1,2] and references therein. Such transition may take place in, e.g., neutron stars; however, the only means to get the nuclear matter under extreme conditions in the laboratory are heavy-ion collisions at (ultra)relativistic energies. Although the first hydrodynamic model of multiparticle production was proposed almost 70 years ago [3], its further modifications have become very popular nowadays because of the successful description of experimental results obtained for heavy-ion collisions at energies of RHIC BNL (up to $\sqrt{s} = 200$ GeV) and LHC CERN (up to $\sqrt{s} = 5.02$ TeV). After analysis of RHIC data, it was announced by all four RHIC collaborations, BRAHMS, PHENIX, PHOBOS and STAR, that the created hot and dense nuclear substance behaved similarly to a perfect fluid [4–7]. At the same time, theoretical calculations of the shear viscosity to entropy density, made within strongly coupled conformal gauge theory by means of the anti-de Sitter/conformal field theory (AdS/CFT) correspondence [8], set the lower limit for this ratio, $\eta/s \geq 1/(4\pi)$, for all physical systems. Additionally, more thorough study of differential elliptic flow v_2 [9,10] of charged particles, produced in A+A collisions at energies of RHIC and LHC, as a function of transverse momentum p_T , has revealed that a small but nonzero value of the ratio η/s is needed for the correct description of the signal at $p_T \geq 2.5$ GeV/c. Recall that for all known substances the shear viscosity over entropy density should reach minimum if the system is in the tricritical point [11].

Since then, the values of η/s began to be intensively estimated. Hydrodynamic models are macroscopic ones; therefore, a dissipative term such as shear viscosity enters the equations of viscous hydrodynamics as an external parameter, which should be

obtained somehow. One way to do so is fitting the calculations performed within the viscous hydrodynamic model, or hybrid model, to the experimental data [12–18]. For the sake of simplicity, these calculations imply the constant ratio of η/s , although several works have tried to take the temperature dependence of this ratio into account [19,20]. The computation of transport coefficients of hadronic systems, consisting of mixture of hadron species, is possible within the microscopic kinetic theory. However, this is a non-trivial task from an analytic point of view [21,22] because one has to know cross-sections of various hadronic collisions and mean fields. Therefore, lattice QCD calculations of η/s are usually done for gluons at zero net baryon density and at temperatures around 160 MeV [23,24]. Microscopic transport models are better suited for such study. In the past, the shear viscosity and its ratio over entropy density were studied in, e.g., the ultra-relativistic quantum molecular dynamics (UrQMD) model [25–29], the parton-hadron-string dynamics (PHSD) model [30], the simulating many accelerated strongly interacting hadrons (SMASH) model [31] and the parton cascade (PC) models to solve various types of Boltzmann collision processes [32–35]. Many of these calculations were performed at conditions corresponding to those of heavy-ion collisions at energies of RHIC and LHC. In this domain, the transition between QGP and hadronic matter is just a smooth crossover.

The modern trend in high-energy physics nowadays is to search for the critical point, at which the deconfinement first-order phase transition becomes a second-order one, at much lower collision energies accessible to the Beam Energy Scan (BES) program at RHIC and at soon-to-open facilities NICA at JINR and FAIR at GSI. Our study is devoted to the beam energies between $E_{lab} = 10$ AGeV and $E_{lab} = 40$ AGeV. In this energy range, the temperature of deconfinement phase transition is expected to be lower compared to that at higher energies, but the baryon chemical potential is quite significant and cannot be neglected. The transition from meson-dominated to baryon-dominated hadronic matter with decreasing beam energy takes place here as well. The main aim of the present paper is to the evolution of partial shear viscosities of the most abundant hadronic species in an expanding and cooling hadronic mixture formed in a symmetric system of centrally colliding gold nuclei. We used the UrQMD model [36,37] and employed the technique developed in [28,29,38]. Section 2 describes the Green–Kubo formalism for determination of the shear viscosity. Within this approach, one has to know the correlator, the relaxation time and the temperature of the system. Determination of these parameters, and baryon chemical potential and strangeness chemical potential, is explained in Section 3. Section 4 presents the calculations of evolution of partial shear viscosity and its ratio over entropy density for nucleons, pions, kaons and $\Lambda + \Sigma$ in the central area of central Au+Au collisions at four different beam energies, $E_{lab} = 10, 20, 30$ and 40 AGeV. Finally, conclusions are drawn in Section 5.

2. Calculation of Shear Viscosity within Green–Kubo Formalism

In classical thermodynamics, one can determine the shear viscosity by means of Chapman–Enskog method [39]. Microscopic transport models, however, allow calculation of the shear viscosity by using the Green–Kubo formalism [40,41] during the study of relaxation process in the disturbed system. Note that the formalism relies on assumption of existence of the equilibrated state. Therefore, one has to study the relaxation of the system to equilibrium before calculation of shear viscosity. The whole formalism is quite straightforward. It is convenient to use Planck, or natural, units: $\hbar = k_B = c = 1$. The shear viscosity in these units is

$$\eta(t_0) = \frac{V}{T} \int_{t_0}^{\infty} \langle \pi(t) \pi(t_0) \rangle_t dt \quad (1)$$

containing the volume V and temperature T of the system, and initial (t_0) and final (t) time of the calculation. The correlator in the integrand reads

$$\langle \pi(t) \pi(t_0) \rangle_t = \lim_{t_{\max} \rightarrow \infty} \frac{1}{t_{\max} - t_0} \int_{t_0}^{t_{\max}} \pi^{ij}(t + t') \pi^{ij}(t') dt' \quad (2)$$

where $\pi^{ij}(t)$ is the non-diagonal part of the energy-momentum tensor T^{ij} .

$$\pi^{ij}(t) = \frac{1}{V} \sum_{k=1}^{\text{particles}} \frac{p_k^i(t)p_k^j(t)}{E_k(t)}. \quad (3)$$

Here $p_k^{i(j)}$ is the $i(j)$ th components of momentum of particle k and E_k is its energy, respectively. The correlator (2) can be approximated by [40,41]

$$\langle \pi(t)\pi(t_0) \rangle_t \approx \langle \pi(t_0)\pi(t_0) \rangle \exp\left(-\frac{t-t_0}{\tau}\right), \quad (4)$$

where τ is the effective relaxation time. By combining Equation (4) with Equation (1), we get the final expression to calculate the shear viscosity:

$$\eta(t_0) = \frac{V\tau}{T} \langle \pi(t_0)\pi(t_0) \rangle. \quad (5)$$

By looking at Equation (5), it becomes clear that, besides of calculation of the correlator, one has to determine simultaneously temperature of the substance T and the relaxation time τ . Since the procedure to define unambiguously temperature of out-of-equilibrium media is absent, it is necessary to check that the hot and dense nuclear matter in an expanding fireball is in the vicinity of the local equilibrium. After that, temperature, relaxation time and the correlator itself should be determined somehow. The algorithm describing all steps in detail is presented in next section.

3. The Three-Component Method

First of all, one has to choose one of the event generators designed for description of nucleus–nucleus interactions in the investigated energy range. For this purpose, we employ the UrQMD model [36,37]. Some very useful data for our study came from a rich table of particles, antiparticles and resonances from the Particle Data Group (PDG) [42] with masses up to 2.25 GeV/c. The UrQMD describes both hadronic and nuclear collisions at energies ranging from one hundred MeV (Bevalac) to several hundred GeV (RHIC) [36,37] and a few TeV (LHC) [43]. Compared to energies of RHIC and LHC, the energy range selected for the present study is rather modest. We studied very central gold–gold collisions, with impact parameter $b = 0$ fm, within the energy interval from $E_{lab} = 10$ to 40 AGeV. This energy range is accessible for the Beam Energy Scan (BES) at RHIC and for planned facilities, such as FAIR and NICA. As was shown in previous studies within the UrQMD [44–47], there is no global equilibrium within the whole volume of the fireball, even in very central heavy-ion collisions because, for instance, the net baryon charge and net strangeness are not uniformly distributed. A local equilibrium, however, is very likely [46,48–51] at least in the central zone of a rapidly expanding fireball. The investigations revealed that the central cubic cell with volume $V = 5 \times 5 \times 5 = 125$ fm³ is appropriate for investigating the process of relaxation to equilibrium of hot and dense nuclear matter produced in relativistic heavy-ion collisions. It is worth mentioning that the picked-up volume should be neither too large to provide uniform distribution of energy density and conserved charges nor too small to contain enough particles. However, the cell is an open system, and hadrons can leave it freely, thereby decreasing its energy density and particle densities. Therefore, to prove that the matter in the cell is in the vicinity of equilibrium, the following procedure was developed; see, e.g., [44,46,49]. Three main parameters characterizing the cell—namely, the energy density, ϵ^{mic} ; the net baryon density, ρ_B^{mic} ; and the net strangeness density, ρ_S^{mic} —were extracted from the microscopic calculations of the fireball evolution. The time step was just $\Delta t = 1$ fm/c. These parameters were inserted into the statistical model (SM) of an ideal hadron gas containing precisely the same set of degrees of freedom as the microscopic model. The set of nonlinear equations reads

$$\epsilon^{mic} = \sum_i \epsilon_i^{SM} \quad (6)$$

$$\rho_B^{mic} = \sum_i B_i n_i^{SM} \quad (7)$$

$$\rho_S^{mic} = \sum_i S_i n_i^{SM}, \quad (8)$$

containing partial energy density ϵ_i^{SM} and partial number density n_i^{SM} of hadron specie “ i ,” and its baryon B_i and strangeness S_i content. Both n_i^{SM} and ϵ_i^{SM} are just first and second moments of the distribution function

$$f(p, m_i) = \left\{ \exp \left(\frac{\epsilon_i - \mu_i}{T} \right) \pm 1 \right\}^{-1}, \quad (9)$$

namely,

$$n_i^{SM} = \frac{g_i}{(2\pi)^3} \int_0^\infty f(p, m_i) d^3 p \quad (10)$$

$$\epsilon_i^{SM} = \frac{g_i}{(2\pi)^3} \int_0^\infty \epsilon_i f(p, m_i) d^3 p \quad (11)$$

where m_i is particle mass and p is its momentum, and g_i is the spin-isospin degeneracy factor. Sign “−” in Equation (9) stands for bosons and sign “+” stands for fermions. The total chemical potential of the hadron is a linear combination of chemical potentials, related to conserved charges in strong interactions, μ_B and μ_S , respectively. It depends on particle’s baryon B_i and strangeness S_i content:

$$\mu_i = B_i \mu_B + S_i \mu_S. \quad (12)$$

As follows in Equations (9)–(12), the ideal gas of hadrons in the statistical model is fully determined by three parameters, temperature, baryon chemical potential and strangeness chemical potential. If partial particle abundances and energy spectra given by the SM are close (within 10% accuracy) to those of the cell in microscopic model’s calculations, one can conclude that the matter in the cell is in the vicinity of local equilibrium. Then, we are able to determine temperature of the system which enters the expression for calculation of shear viscosity.

However, this is not a full story yet, because we have to determine both the correlator $\langle \pi(t_0) \pi(t_0) \rangle$ and the effective relaxation time τ . This study cannot be done within the analysis of an open system, such as our cell, because of permanently changing conditions in the cell. These conditions must be fixed somehow. Therefore, the third component of the scheme is the box with periodic boundary conditions [52–54] preserving both the total energy and the net baryon and net strangeness composition. Namely, the particles are free to leave the box; however, other particles with the same characteristics (masses, momenta, quantum numbers) enter the box immediately. Elastic and inelastic interactions of hadrons in the box proceed similarly to those in model generated hadronic or nuclear collisions.

The volume of the box can be $V_{box} = 5 \times 5 \times 5 = 125 \text{ fm}^3$, similar to that of the central cell, or larger—e.g., $V_{box} = 10 \times 10 \times 10 = 1000 \text{ fm}^3$ —to reduce the fluctuation effects. The box is initialized with the values of energy density, net baryon density and net strangeness density, which are extracted from the cell at a certain moment. Its initial hadron composition consists usually of protons and neutrons with the admixture (in case of nonzero strangeness density) of kaons or Lambdas. It is worth noting that the relaxation process to a stationary state in the box is quite long; see [52,53]. The typical time scale for the box calculations is about 1000–2000 fm/c. One can study the relaxation process and determine both the correlator(s) and relaxation time τ .

The method developed for determination of shear viscosity in microscopic calculations consists of three steps. The first step includes the generation of heavy ion collisions within the microscopic transport model; determination of volume, in which the occurrence of a local equilibrium is expected; and extraction of three key parameters, i.e., energy density, net baryon density and net strangeness density, out of it. These three parameters are used as an input for the statistical model of ideal hadron gas. This is the second step of the proposed scheme. If the partial yields of hadrons and their energy spectra in the selected volume are close to those given by the SM, one can conclude that the matter is in the vicinity of a local equilibrium. The SM provides us with the values of thermodynamic characteristics, such as temperature, baryon chemical potential and strangeness chemical potential. At the third step we use the extracted values of ϵ , ρ_B and ρ_S to initialize the box with periodic boundary conditions. The correlators and the relaxation times are determined during the study of the matter evolution in the box towards equilibrium.

4. Results: Total and Partial Shear Viscosity of Hadrons

Version 3.4 of the UrQMD model in default cascade mode was employed. Calculations were performed for central gold–gold collisions at four beam energies, $E_{lab} = 10, 20, 30$ and 40 AGeV. At each energy, ca. 50 thousand collisions were generated. Figure 1 displays the evolution of energy density (a), net baryon density (b) and net strangeness density (c) in the central cubic cell of the collision with volume $V = 125$ fm 3 .

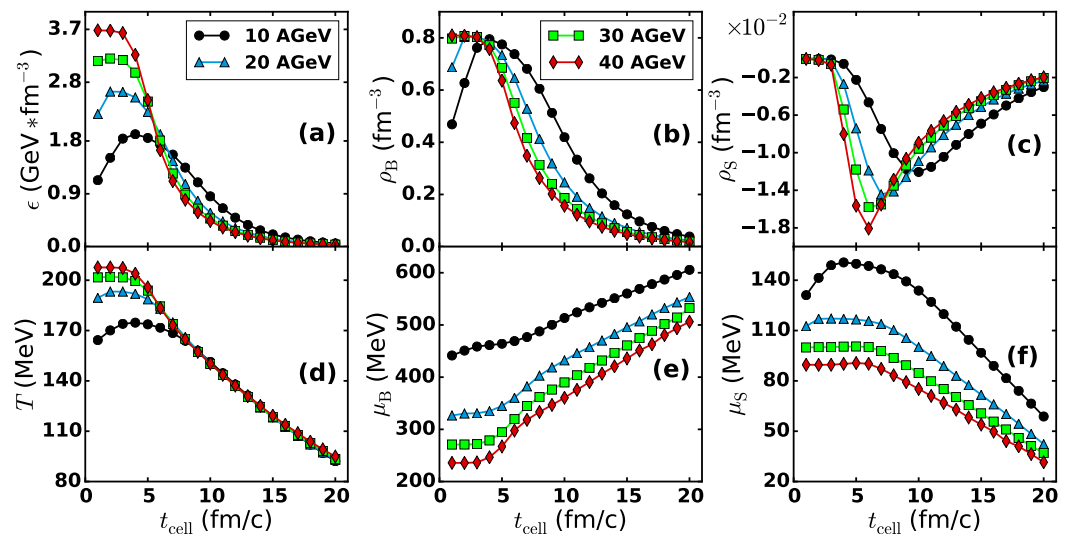


Figure 1. Distributions of (a) energy density, ϵ ; (b) net baryon density, ρ_B ; and (c) net strangeness density, ρ_S , of central Au+Au collisions generated within UrQMD model at $E_{lab} = 10$ AGeV (black circles), 20 AGeV (blue triangles), 30 AGeV (green squares) and 40 AGeV (red diamonds) in the central cell, 125 fm 3 in size. The values of (d) temperature, T ; (e) baryochemical potential, μ_B ; and (f) strangeness chemical potential, μ_S were calculated from the fit to SM of ideal hadron gas. Lines were drawn to guide the eye (From [29]).

We can see that at early times, $t \leq 5$ fm/ c , the energy density in the cell is larger for collisions with larger bombarding energies. However, both remnants of colliding nuclei and very energetic particles leave the central area quickly. After $t \approx 6$ fm/ c , the drop of energy density proceeds with similar rates for all four energies. Net baryon density drops with time also, but here one can observe the clear energy dependence: the lower the beam energy, the higher the net baryon density. The net strangeness density in the cell is small, though negative, at $1 \leq t \leq 20$ fm/ c , as shown in Figure 1c, in line with the previous results; see, e.g., [38,46,49]. This fact can be explained by different cross-sections of positive and negative kaons in baryon-dominated medium. After that, we acquired the temperatures (Figure 1d), baryon chemical potential (Figure 1e) and strangeness chemical potential (Figure 1f) of an ideal hadron gas by inserting the extracted values of ϵ , ρ_B and ρ_S into the

SM equations. Note that matter in the cell reaches chemical and thermal equilibrium in the investigated energy range not earlier than after $t = 6\text{--}8 \text{ fm}/c$. Therefore, parameters T, μ_B, μ_S obtained at earlier times should be treated with great care. It is interesting that at $t \geq 7 \text{ fm}/c$ and until $t = 20 \text{ fm}/c$, temperatures in the cell shown in Figure 1d coincide for the studied beam energies. Baryon chemical potentials, shown in Figure 1e, increase with time, whereas chemical potentials of strangeness decrease, as displayed in Figure 1f.

As was shown in [28], shear viscosity in the box calculations reveals a remarkable plateau for initial times (see Equation (2), $200 \text{ fm}/c \leq t_0 \leq 800 \text{ fm}/c$). The extracted values of η averaged over the plateau are shown in Figure 2. It is worth mentioning that, because of the high number of events used for the box generation at each timestep and averaging over the plateau, the statistical errors in this figure and in the subsequent ones are less than the symbol sizes. Data points corresponding to early times in the cell, $\tau_{cell} \leq 6 \text{ fm}/c$, are connected by the dashed lines. At these times the energy density in the cell is not distributed evenly throughout the cell volume, and hadron abundances and energy spectra, compared to these of the SM of ideal hadron gas, indicate that the matter in the cell is still out of equilibrium [46,49]. Determination of shear viscosity in the cell at $t \leq 6 \text{ fm}/c$ is, therefore, ambiguous. However, when remnants of colliding nuclei and most energetic particles leave the cell, the chemical and thermal equilibrium sets in quickly. One can see that all four distributions $\eta(t_{cell})$ sit practically on the top of each other at $7 \text{ fm}/c \leq t \leq 20 \text{ fm}/c$, fully resembling the temperature drop shown in Figure 1d. The explanation of the decrease in η is as follows. After $t = 6 \text{ fm}/c$, inelastic collisions in the cell rapidly cease, and (quasi)elastic interactions start to dominate. The soft scattering modes quickly redistribute the energy and momentum of hadrons, which leads to a decrease in the relaxation time τ , and consequently, the shear viscosity in the cell.

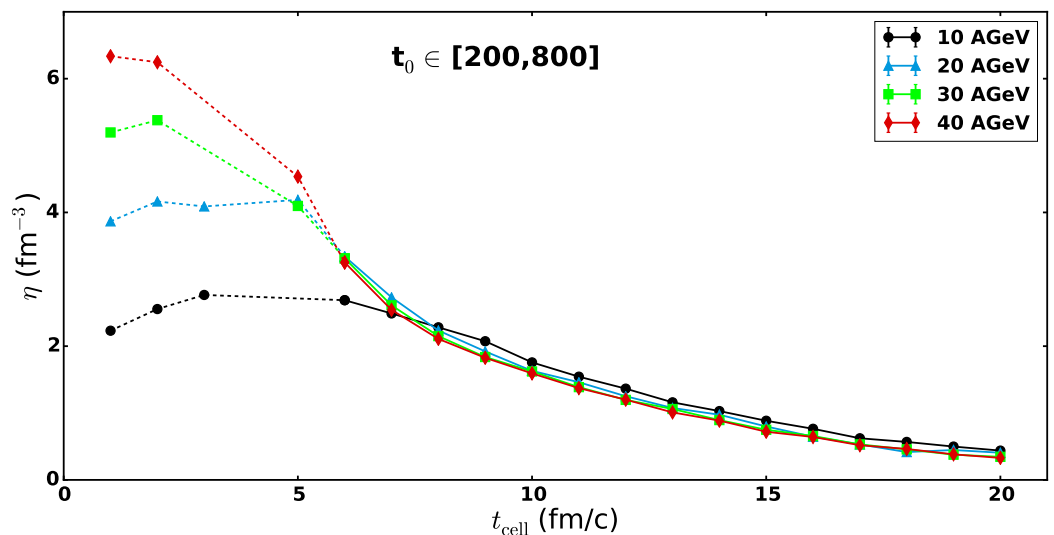


Figure 2. Shear viscosity of hadrons in the UrQMD box with initial conditions corresponding to those of the central cell of UrQMD-generated central Au+Au collisions at $E_{lab} = 40 \text{ AGeV}$ (red diamonds), 30 AGeV (green squares), 20 AGeV (blue triangles) and 10 AGeV (black circles). Dashed lines indicate the out-of-equilibrium stage, whereas solid lines correspond to the (nearly) equilibrium stage. See text for details.

In what follows, we study the partial shear viscosities of the main hadron species in the central cell, namely, nucleons, pions, kaons and $\Lambda + \Sigma$, and the combined viscosities of baryons and mesons. This means that only the correlators for the appropriate type of hadrons, e.g., $\langle \pi^N \pi^N \rangle$, are considered. The analysis of the thermodynamic conditions in the cell starts from time $t = 8 \text{ fm}/c$ when the hadronic matter is close to thermal and chemical equilibrium. Shear viscosity of nucleons in Au+Au collisions at all four beam energies is shown in Figure 3. It smoothly decreases with time, and therefore, with temperature for all

reactions. Additionally, the lower the energy of nuclear collision, the higher the nucleon's shear viscosity. Since temperatures in the cell after $t = 8 \text{ fm}/c$ are practically the same at different timesteps for all four beam energies, the difference in η values can be attributed to different values of baryon chemical potential and to dominance of baryon fraction in the particle spectrum.

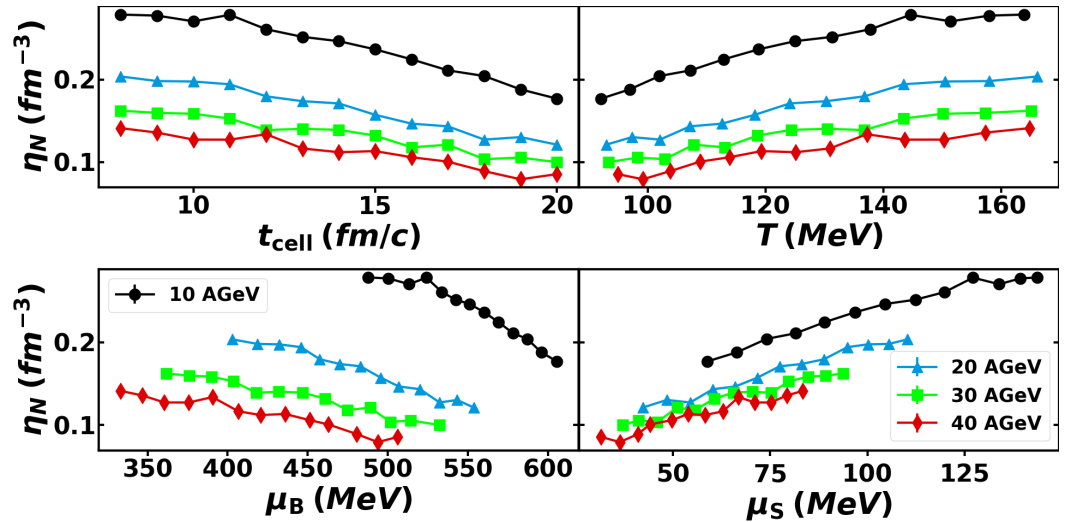


Figure 3. Upper row: Shear viscosity of nucleons, η^N , calculated in the central cell as function of time t_{cell} after the beginning of nuclear collision (left), and temperature T of the cell (right). Bottom row: The same as the upper one but for baryon chemical potential, μ_B , (left) and for strangeness chemical potential, μ_S , (right). Beam energies and labeling of the curves are the same as in Figure 1.

The partial shear viscosity of the combined spectrum of Lambdas and Sigmas, displayed in Figure 4, also demonstrates this tendency, although very weak. The calculated distributions $\eta^{\Lambda+\Sigma}(t_{cell})$ and $\eta^{\Lambda+\Sigma}(T)$ are close to each other within the studied energy range. One can see also that the values of shear viscosity of $\Lambda + \Sigma$ hyperons are almost two times lower compared to those of nucleons. The plausible explanation is that the yield of hyperons in Au+Au collisions at $10 \text{ AGeV} \leq E_{lab} \leq 40 \text{ AGeV}$ is relatively low. Therefore, hyperons interact mainly with other hadrons and the genuine correlation between them is lost quite early.

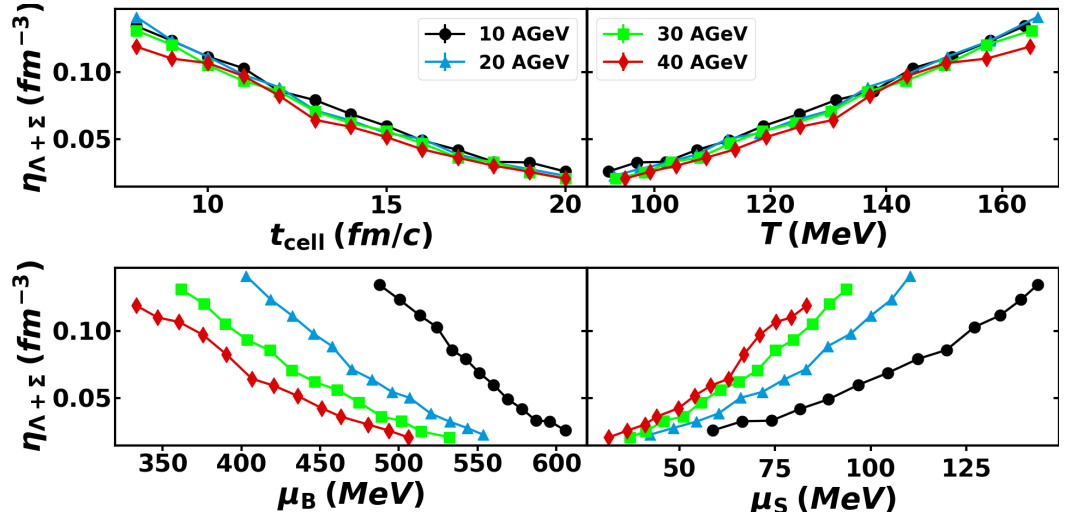


Figure 4. The same as Figure 3 but for shear viscosity of $\Lambda + \Sigma$.

Pions are the most abundant mesons among the produced particles. In contrast to nucleons, the partial shear viscosity of pions drops with decreasing beam energy for the

distributions $\eta^\pi(t_{cell})$ and $\eta^\pi(T)$, as shown in Figure 5. Recall that temperatures in the cell at all four energies are almost the same within the time interval $8 \leq t_{cell} \leq 20 \text{ fm}/c$, and that pions are not affected by chemical potentials of the baryon charge and strangeness. The spectrum of hadrons in heavy-ion collisions at low and intermediate energies is dominated by baryons, and less pions are produced at lower energies. The decrease in pion shear viscosity with time in the cell proceeds faster compared to that of the nucleon one.

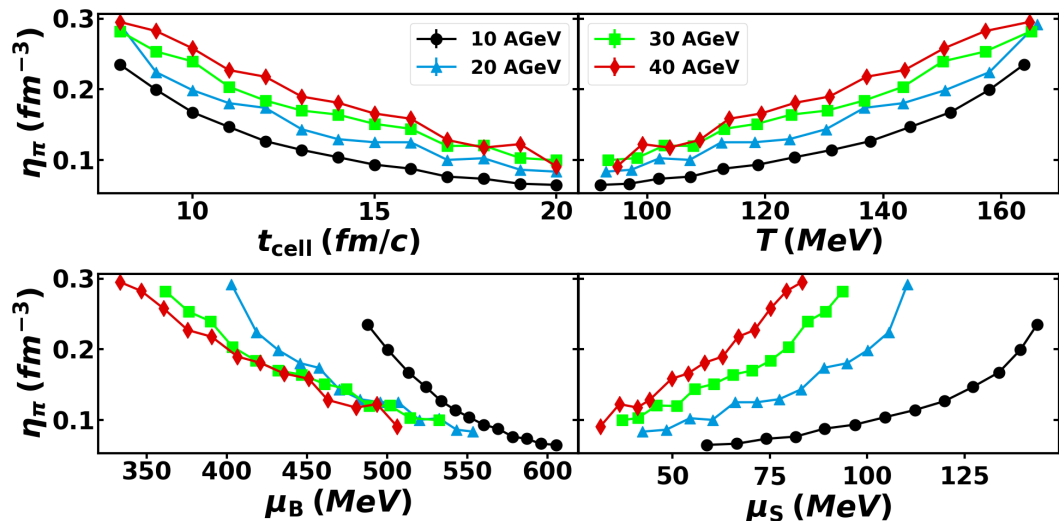


Figure 5. The same as Figure 3 but for shear viscosity of pions.

The next group of mesons in particle spectrum is kaons. Figure 6 displays their shear viscosity in the central cell. Here, one can see no difference between $\eta^K(t_{cell})$ and $\eta^K(T)$ for beam energies between 10 and 40 AGeV despite the different strangeness chemical potentials. It seems that chemical potentials play a minor role in the (partial) shear viscosity of hadrons. The latter is mainly determined by temperature of the system and particle abundances.

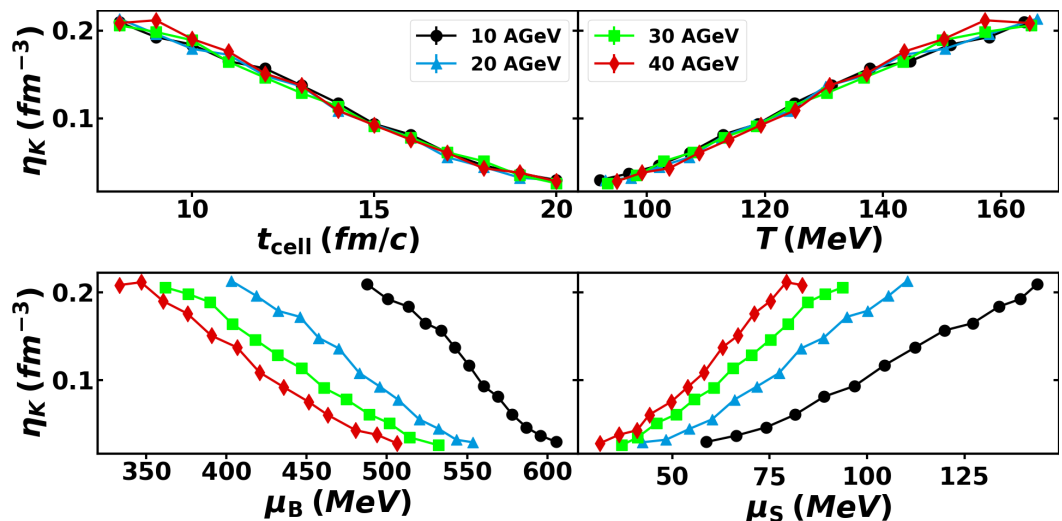


Figure 6. The same as Figure 3 but for shear viscosity of kaons.

The combined shear viscosity of baryons in the central cell is presented in Figure 7, and Figure 8 shows that of mesons. Both figures reveal the same trends observed earlier for individual hadron distributions. Namely, the shear viscosities of both baryons and mesons, in the central cell drop with time, and therefore, with decreasing energy density and temperature of the cell. However, for baryons the shear viscosity increases with decreasing beam energy, whereas shear viscosity of mesons demonstrates the opposite tendency. When the beam energy goes down from $E_{lab} = 40$ to 20 AGeV, the difference in meson or baryon shear viscosities for neighbor beam energies is about 10% or less. Note also that at $E_{lab} \approx 30$ AGeV the partial shear viscosities of baryons and mesons are about the same. Significant rise of $\eta^{baryons}$ is observed at $E_{lab} = 10$ AGeV; see Figure 7. Here the total spectrum of hadrons is heavily dominated by baryons.

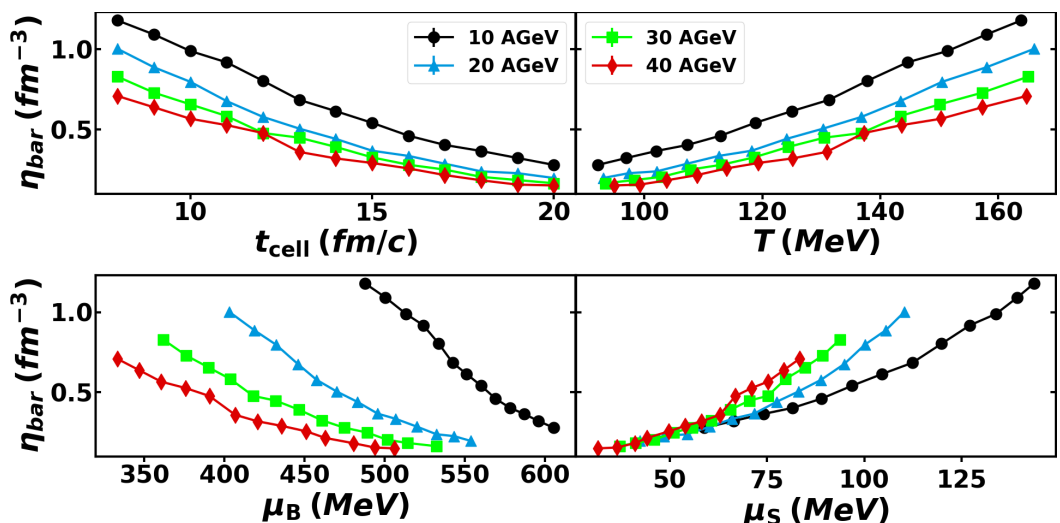


Figure 7. The same as Figure 3 but for combined shear viscosity of baryons.

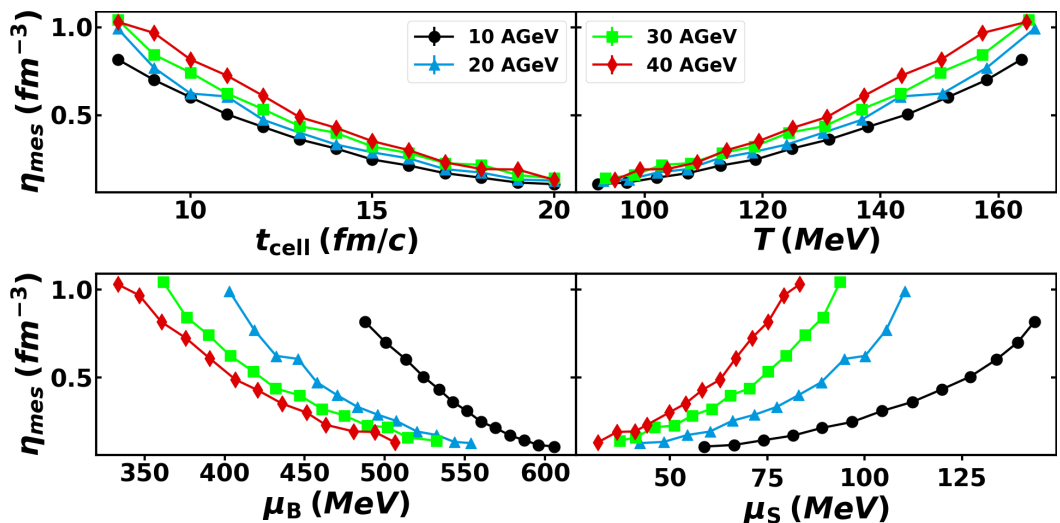


Figure 8. The same as Figure 7 but for combined shear viscosity of mesons.

This energy range is very interesting. If heavy ions are colliding with the beam energies of hundred MeV, one deals merely with hadrons and their excited states, resonances. When the energy of nuclear collisions increases to several GeV, new objects, called strings, come into play. Strings are not hadrons and can be considered as precursors of quark-gluon plasma. With a further increase in bombarding energy, mesons (mainly, pions) become the most abundant part of the hadronic spectrum, and therefore, a transition from baryon-dominated to meson-dominated matter takes place. Thus, it is important to check the

possible fingerprints of these transitions on the ratio of shear viscosity to entropy density. The latter is determined in the SM for a hadronic specie “i” as

$$s_i = -\frac{g_i}{2\pi^2} \int_0^\infty f(p, m_i) [\ln f(p, m_i) - 1] p^2 dp , \quad (13)$$

Bearing in mind the ratio limit $\eta/s \geq 1/4\pi$ [8], we plotted the ratio $4\pi\eta/s$ for all hadrons as a function of t_{cell} , T , μ_B and μ_S in Figure 9. One can see that this ratio for all hadrons in the system decreases with decreasing beam energy of Au+Au collisions. However, even for the collisions with $E_{lab} = 10$ AGeV the minimum of $4\pi\eta/s$ is four times larger than unity. It is worth mentioning that open symbols in Figure 9 indicate the results obtained at early times for out-of-equilibrium stage. These results, therefore, are ambiguous and should be treated with great care, and the indications on shallow minima of η/s around $t_{cell} \sim 5$ fm/c.

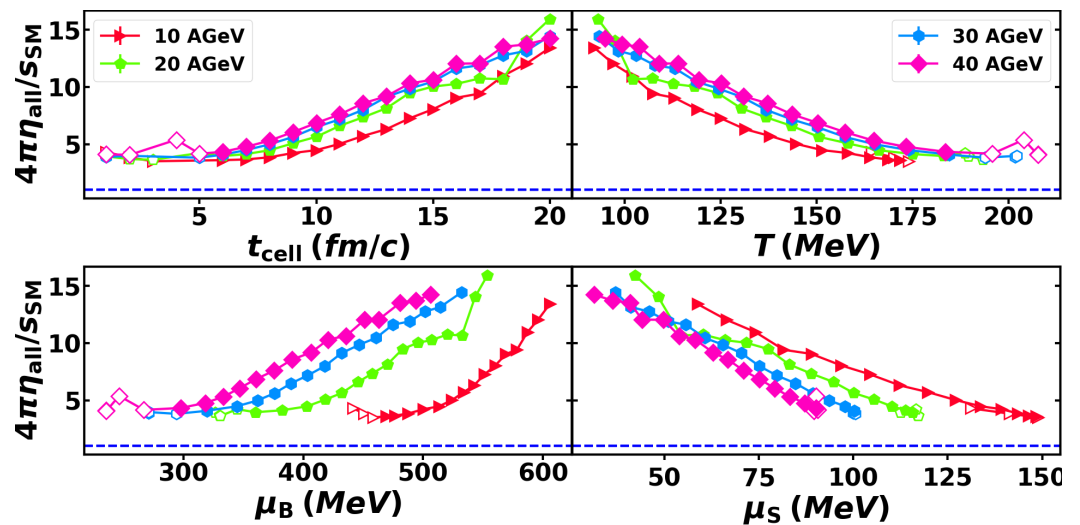


Figure 9. The same as Figure 8 but for ratio of total shear viscosity of hadrons to their entropy density, $4\pi\eta/s$.

A direct comparison of the obtained results with the results of other models is difficult, since the latter were obtained at a constant (most often, zero) value of the baryon chemical potential. The general trend, however, is qualitatively correct. The ratio of the shear viscosity over the entropy density increases (i) with decreasing temperature and (ii) with increasing baryon chemical potential. A more detailed comparison of the predictions of different models can be found in [31].

The last step is to study the partial contributions of baryons and mesons to η/s ratio. Figures 10 and 11 display the ratios $4\pi\eta^{baryons}/s$ and $4\pi\eta^{mesons}/s$, respectively. Figure 10 indicates that the evolution of partial ratio η/s for baryons in the cell at $8 \text{ fm}/c \leq t_{cell} \leq 20 \text{ fm}/c$ proceeds similarly for all four beam energies. However, a very weak rise in this ratio with dropping beam energy seems to take place. The reduction in the ratio of total shear viscosity to entropy density in the medium is caused by the decreased contribution of mesons, as shown in Figure 11. In stark contrast to baryons, the mesonic ratio η^{mesons}/s demonstrates distinct separation in terms of temperature and chemical potentials. Note also that this ratio varies slightly in the cell within the considered time interval.

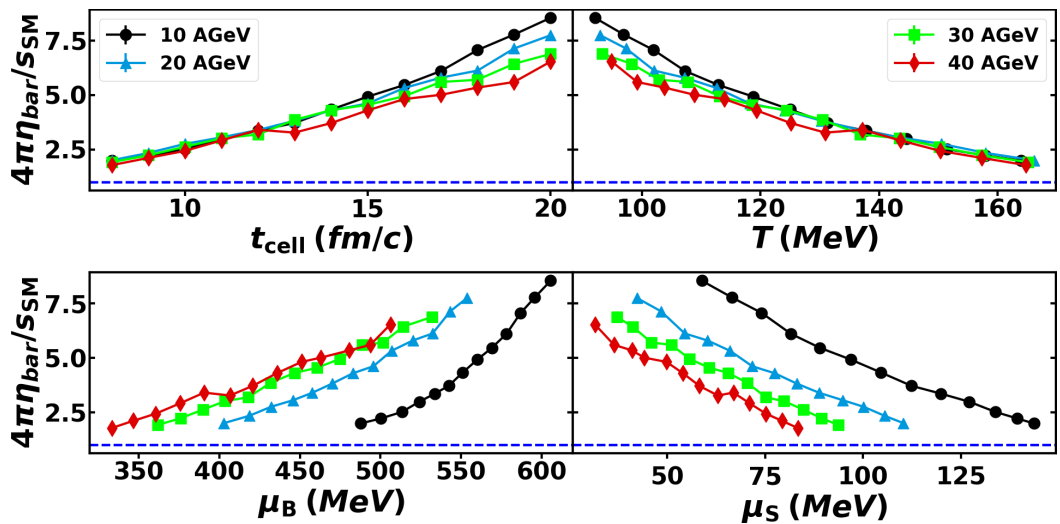


Figure 10. The same as Figure 9 but for shear viscosity of baryons to the entropy density ratio.

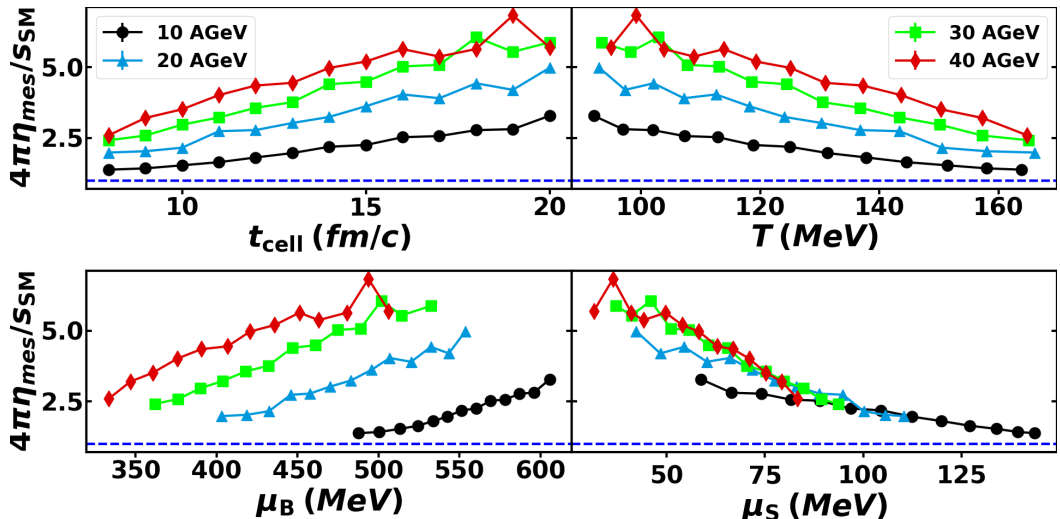


Figure 11. The same as Figure 10 but for shear viscosity of mesons to the entropy density ratio.

5. Discussion and Conclusions

We studied evolution of shear viscosity η of hot and dense nuclear matter produced in the central area of gold–gold collisions at beam energies ranging from $E_{lab} = 10$ to 40 AGeV. The main goal was to study the partial contributions to η of main hadron species, such as nucleons, pions, kaons and lambdas/sigmas. The general procedure for determination of the shear viscosity in microscopic transport calculations consists of three main parts; see, e.g., [28,29]. Firstly, a central cubic cell 125 fm^3 in size was selected. Then, energy density, net baryon density and net strangeness density in the cell were determined. Secondly, our statistical model of ideal hadron gas employed the extracted values of $\varepsilon, \rho_B, \rho_S$ to determine temperature T , baryon chemical potential μ_B and strangeness chemical potential μ_S of hadron resonance gas in thermal and chemical equilibrium. If the yields and energy spectra of hadronic species in microscopic calculations are close to those given by the SM, the matter in the cell can be considered to be in the vicinity of local equilibrium. Thus, one gets T, μ_B and μ_S of the system. Third, we determined the shear viscosity of the system with the Green–Kubo approach. To do this, one has to initialize the box with periodic boundary conditions with essentially the same values of $\varepsilon, \rho_B, \rho_S$ as given by the cell calculations at each time snapshot.

The obtained physical results can be summarized as follows. Temperatures in the central cell at each time step between $t = 8 \text{ fm}/c$ and $t = 20 \text{ fm}/c$ are similar for all four

energies. The total shear viscosities in the central areas of the four different reactions are also similar within this time interval. Partial shear viscosities, however, demonstrate different tendencies. The lower the beam energy, the higher the nucleon shear viscosity. Hyperons $\Lambda + \Sigma$ also reveal this trend, but to a much lesser extent. In contrast, shear viscosity of pions decreases with decreasing beam energy, whereas kaon shear viscosity is almost independent on the beam energy within the investigated interval. The contributions of baryons and mesons to the total shear viscosity are approximately the same at beam energy 30 AGeV. At higher and lower beam energies, this symmetry between the baryon and the meson sectors is broken. The ratio of shear viscosity of hadrons to their entropy density also declines with decreasing collision energy. This drop is attributed to mesons. For baryons, the distributions of $\eta^{baryons}/s(t_{cell})$ increase slightly, though remaining very close to each other, with dropping E_{lab} . Our results might be useful also for the development of sophisticated hydrodynamic models for heavy-ion collisions at intermediate energies.

Author Contributions: Investigation, methodology, software and visualization, M.T.; conceptualization, methodology and supervision, L.B.; conceptualization, investigation, methodology and writing—original draft, E.Z. All authors have read and agreed to the published version of the manuscript.

Funding: The work was supported by the Norwegian Centre for International Cooperation in Education (SIU) under grants “CPEA-LT-2016/10094—From Strong Interacting Matter to Dark Matter” and “UTF-2016-long-term/10076—Training of Bachelor, Master and PhD Students specialized in high energy physics.” The work of L.B. and E.Z. was supported by the Norwegian Research Council (NFR) under grant 255253/F50—“CERN Heavy Ion Theory,” and by the Russian Foundation for Basic Research (RFBR) under grants 18-02-40084 and 18-02-40085.

Institutional Review Board Statement: Not applicable.

Informed Consent Statement: Not applicable.

Data Availability Statement: Not applicable.

Acknowledgments: Fruitful discussions with L.P. Csnerai and K. Tywoniuk are gratefully acknowledged. All computation were performed at Govorun (JINR, Dubna) cluster facility.

Conflicts of Interest: The authors declare no conflict of interest.

References

1. Sarkar, S.; Satz, H.; Sinha, B. *The Physics of the Quark-Gluon Plasma: Introductory Lectures*; Lecture Notes in Physics; Springer: Berlin/Heidelberg, Germany, 2010; Volume 785, pp. 1–369. [[CrossRef](#)]
2. *Proceedings of Quark Matter 2019*; Liu, F., Wang, E., Wang, X.-N., Xu, N., Zhang, B.-W., Eds.; Nuclear Physics A; Elsevier: Amsterdam, The Netherlands, 2021; Volume 1005.
3. Landau, L.D. On the multiparticle production in high-energy collisions. *Izv. Akad. Nauk. Ser. Fiz.* **1953**, *17*, 51–64.
4. Arsene, I.; Bearden, I.; Beavis, D.; Besliu, C.; Budick, B.; Bøggild, H.; Chasman, C.; Christensen, C.; Christiansen, P.; Cibor, J.; et al. Quark gluon plasma and color glass condensate at RHIC? The Perspective from the BRAHMS experiment. *Nucl. Phys. A* **2005**, *757*, 1–27. [[CrossRef](#)]
5. Back, B.; Baker, M.; Ballintijn, M.; Barton, D.; Becker, B.; Betts, R.; Bickley, A.; Bindel, R.; Budzanowski, A.; Busza, W.; et al. The PHOBOS perspective on discoveries at RHIC. *Nucl. Phys. A* **2005**, *757*, 28–101. [[CrossRef](#)]
6. Adams, J.; Aggarwal, M.; Ahammed, Z.; Amonett, J.; Anderson, B.; Arkhipkin, D.; Averichev, G.; Badyal, S.; Bai, Y.; Balewski, J.; et al. Experimental and theoretical challenges in the search for the quark gluon plasma: The STAR Collaboration’s critical assessment of the evidence from RHIC collisions. *Nucl. Phys. A* **2005**, *757*, 102–183. [[CrossRef](#)]
7. Adcox, K.; Adler, S.; Afanasiev, S.; Aidala, C.; Ajitanand, N.; Akiba, Y.; Al-Jamel, A.; Alexander, J.; Amirikas, R.; Aoki, K.; et al. Formation of dense partonic matter in relativistic nucleus-nucleus collisions at RHIC: Experimental evaluation by the PHENIX collaboration. *Nucl. Phys. A* **2005**, *757*, 184–283. [[CrossRef](#)]
8. Kovtun, P.; Son, D.T.; Starinets, A.O. Viscosity in strongly interacting quantum field theories from black hole physics. *Phys. Rev. Lett.* **2005**, *94*, 111601. [[PubMed](#)]
9. Ollitrault, J.-Y. Anisotropy as a signature of transverse collective flow. *Phys. Rev. D* **1992**, *46*, 229–245. [[PubMed](#)]
10. Poskanzer, A.M.; Voloshin, S.A. Methods for analyzing anisotropic flow in relativistic nuclear collisions. *Phys. Rev. C* **1998**, *58*, 1671–1678. [[CrossRef](#)]

11. Csernai, L.P.; Kapusta, J.I.; McLerran, L.D. On the Strongly-Interacting Low-Viscosity Matter Created in Relativistic Nuclear Collisions. *Phys. Rev. Lett.* **2006**, *97*, 152303. [[CrossRef](#)]
12. Romatschke, P.; Romatschke, U. Viscosity Information from Relativistic Nuclear Collisions: How Perfect is the Fluid Observed at RHIC? *Phys. Rev. Lett.* **2007**, *99*, 172301. [[CrossRef](#)]
13. Dusling, K.; Teaney, D. Simulating elliptic flow with viscous hydrodynamics. *Phys. Rev. C* **2008**, *77*, 034905. [[CrossRef](#)]
14. Schenke, B.; Tribedy, P.; Venugopalan, R. Fluctuating Glasma initial conditions and flow in heavy ion collisions. *Phys. Rev. Lett.* **2012**, *108*, 252301. [[CrossRef](#)] [[PubMed](#)]
15. Schenke, B.; Tribedy, P.; Venugopalan, R. Event-by-event gluon multiplicity, energy density, and eccentricities in ultrarelativistic heavy-ion collisions. *Phys. Rev. C* **2012**, *86*, 034908. [[CrossRef](#)]
16. Karpenko, I.A.; Huovinen, P.; Petersen, H.; Bleicher, M. Estimation of the shear viscosity at finite net-baryon density from A+A collision data at $\sqrt{s_{NN}} = 7.7 - 200$ GeV. *Phys. Rev. C* **2015**, *91*, 064901. [[CrossRef](#)]
17. Ivanov, Y.B.; Soldatov, A.A. Entropy Production and Effective Viscosity in Heavy-Ion Collisions. *Eur. Phys. J. A* **2016**, *52*, 367. [[CrossRef](#)]
18. Ivanov, Y.B.; Soldatov, A.A. Estimation of the shear viscosity from 3FD simulations of Au + Au collisions at $\sqrt{s_{NN}} = 3.3 - 39$ GeV. *Eur. Phys. J. A* **2016**, *52*, 117. [[CrossRef](#)]
19. Song, H.; Bass, S.A.; Heinz, U. Viscous QCD matter in a hybrid hydrodynamic+Boltzmann approach. *Phys. Rev. C* **2011**, *83*, 024912. [[CrossRef](#)]
20. Niemi, H.; Denicol, G.S.; Huovinen, P.; Molnar, E.; Rischke, D.H. Influence of a temperature-dependent shear viscosity on the azimuthal asymmetries of transverse momentum spectra in ultrarelativistic heavy-ion collisions. *Phys. Rev. C* **2012**, *86*, 014909. [[CrossRef](#)]
21. Chakraborty, P.; Kapusta, J.I. Quasi-Particle Theory of Shear and Bulk Viscosities of Hadronic Matter. *Phys. Rev. C* **2011**, *83*, 014906. [[CrossRef](#)]
22. Noronha-Hostler, J.; Noronha, J.; Greiner, C. Hadron Mass Spectrum and the Shear Viscosity to Entropy Density Ratio of Hot Hadronic Matter. *Phys. Rev. C* **2012**, *86*, 024913. [[CrossRef](#)]
23. Meyer, H.B. A Calculation of the shear viscosity in SU(3) gluodynamics. *Phys. Rev. D* **2007**, *76*, 101701. [[CrossRef](#)]
24. Astrakhantsev, N.; Braguta, V.; Kotov, A. Temperature dependence of shear viscosity of SU(3)-gluodynamics within lattice simulation. *J. High Energy Phys.* **2017**, *4*, 101. [[CrossRef](#)]
25. Muronga, A. Shear viscosity coefficient from microscopic models. *Phys. Rev. C* **2004**, *69*, 044901. [[CrossRef](#)]
26. Demir, N.; Bass, S.A. Shear-Viscosity to Entropy-Density Ratio of a Relativistic Hadron Gas. *Phys. Rev. Lett.* **2009**, *102*, 172302. [[CrossRef](#)] [[PubMed](#)]
27. Motornenko, A.; Bravina, L.; Gorenstein, M.I.; Mager, A.G.; Zabrodin, E. Nucleon matter equation of state, particle number fluctuations, and shear viscosity within UrQMD box calculations. *J. Phys. G* **2018**, *45*, 035101. [[CrossRef](#)]
28. Teslyk, M.; Bravina, L.; Panova, O.; Vitiuk, O.; Zabrodin, E. Shear viscosity in microscopic calculations of A+A collisions at energies available at the Nuclotron-based Ion Collider fAcility (NICA). *Phys. Rev. C* **2020**, *101*, 014904. [[CrossRef](#)]
29. Zabrodin, E.; Teslyk, M.; Vitiuk, O.; Bravina, L. Calculation of shear viscosity in Au+Au collisions at NICA energies. *Phys. Scr.* **2020**, *85*, 074009. [[CrossRef](#)]
30. Ozvenchuk, V.; Linnyk, O.; Gorenstein, M.I.; Bratkovskaya, E.L.; Cassing, W. Shear and bulk viscosities of strongly interacting “infinite” parton-hadron matter within the parton-hadron-string dynamics transport approach. *Phys. Rev. C* **2013**, *87*, 064903. [[CrossRef](#)]
31. Rose, J.B.; Torres-Rincon, J.M.; Schäfer, A.; Oliinychenko, D.R.; Petersen, H. Shear viscosity of a hadron gas and influence of resonance lifetimes on relaxation time. *Phys. Rev. C* **2018**, *97*, 055204. [[CrossRef](#)]
32. Xu, Z.; Greiner, C.; Stoecker, H. PQCD calculations of elliptic flow and shear viscosity at RHIC. *Phys. Rev. Lett.* **2008**, *100*, 172301. [[CrossRef](#)]
33. Plumari, S.; Puglisi, A.; Scardina, F.; Greco, V. Shear viscosity of a strongly interacting system: Green-Kubo correlator versus Chapman-Enskog and relaxation-time approximations. *Phys. Rev. C* **2012**, *86*, 054902. [[CrossRef](#)]
34. Wesp, C.; El, A.; Reining, F.; Xu, Z.; Bouras, I.; Greiner, C. Calculation of shear viscosity using Green-Kubo relations within a parton cascade. *Phys. Rev. C* **2011**, *84*, 054911. [[CrossRef](#)]
35. Rais, J.; Gallmeister, K.; Greiner, C. The shear viscosity to entropy density ratio in Hagedorn states. *Phys. Rev. D* **2020**, *102*, 036009. [[CrossRef](#)]
36. Bass, S.A. Microscopic models for ultrarelativistic heavy ion collisions. *Prog. Part. Nucl. Phys.* **1998**, *41*, 255–369. [[CrossRef](#)]
37. Bleicher, M.; Zabrodin, E.; Spieles, C.; Bass, S.; Ernst, C.; Soff, S.; Bravina, L.; Belkacem, M.; Weber, H.; Stöcker, H.; et al. Relativistic hadron hadron collisions in the ultrarelativistic quantum molecular dynamics model. *J. Phys. G* **1999**, *25*, 1859–1896. [[CrossRef](#)]
38. Zabrodin, E.; Bravina, L.; Teslyk, M.; Vitiuk, O. Early thermalization and shear viscosity to entropy ratio in heavy-ion collisions at energies of BES, FAIR and NICA. *Nucl. Phys. A* **2021**, *1005*, 121861. [[CrossRef](#)]
39. De Groot, S.R.; van Leeuwen, W.A.; Weert, C. *Relativistic Kinetic Theory, Principles and Applications*; North-Holland Publishing Company: Amsterdam, The Netherlands, 1980.
40. Green, M.S. Markoff Random Processes and the Statistical Mechanics of Time-Dependent Phenomena. II. Irreversible Processes in Fluids. *J. Chem. Phys.* **1954**, *22*, 398. [[CrossRef](#)]

41. Kubo, R. Statistical-Mechanical Theory of Irreversible Processes. I. General Theory and Simple Applications to Magnetic and Conduction Problems. *J. Phys. Soc. Jpn.* **1957**, *12*, 570–586. [[CrossRef](#)]
42. Tanabashi, M.; Hagiwara, K.; Hikasa, K.; Nakamura, K.; Sumino, Y.; Takahashi, F.; Tanaka, J.; Agashe, K.; Aielli, G.; Amsler, C.; et al. Review of Particle Physics. *Phys. Rev. D* **2018**, *98*, 030001. [[CrossRef](#)]
43. Mitrovski, M.; Schuster, T.; Gräf, G.; Petersen, H.; Bleicher, M. Charged particle (pseudo-)rapidity distributions in $p + \bar{p} / p + p$ and Pb+Pb/Au+Au collisions from UrQMD calculations at energies available at the CERN Super Proton Synchrotron to the Large Hadron Collider. *Phys. Rev. C* **2009**, *79*, 044901. [[CrossRef](#)]
44. Bravina, L.; Gorenstein, M.; Belkacem, M.; Bass, S.; Bleicher, M.; Brandstetter, M.; Hofmann, M.; Soff, S.; Spieles, C.; Weber, H.; et al. Local thermodynamical equilibrium and the equation of state of hot, dense matter created in Au+Au collisions at AGS. *Phys. Lett. B* **1998**, *434*, 379–387. [[CrossRef](#)]
45. Bravina, L.; Gorenstein, M.; Belkacem, M.; Bass, S.; Bleicher, M.; Brandstetter, M.; Hofmann, M.; Soff, S.; Spieles, C.; Weber, H.; et al. Local thermal and chemical equilibration and the equation of state in relativistic heavy ion collisions. *J. Phys. G* **1999**, *25*, 351–362. [[CrossRef](#)]
46. Bravina, L.V.; Brandstetter, M.; Gorenstein, M.I.; Zabrodin, E.E.; Belkacem, M.; Bleicher, M.; Bass, S.; Ernst, C.; Hofmann, M.; Soff, S.; et al. Local equilibrium in heavy ion collisions: Microscopic model versus statistical model analysis. *Phys. Rev. C* **1999**, *60*, 024904. [[CrossRef](#)]
47. Bravina, L.V.; Zabrodin, E.E.; Gorenstein, M.I.; Bass, S.; Belkacem, M.; Bleicher, M.; Brandstetter, M.; Ernst, C.; Hofmann, M.; Neise, L.; et al. Chemical freezeout parameters at RHIC from microscopic model calculations. *Nucl. Phys. A* **2002**, *698*, 383–386. [[CrossRef](#)]
48. Bravina, L.V.; Zabrodin, E.E.; Bass, S.; Faessler, A.; Fuchs, C.; Gorenstein, M.I.; Greiner, W.; Soff, S.; Stöcker, H.; Weber, H. Equation of state of resonance rich matter in the central cell in heavy ion collisions at $S^{1/2} = 200$ AGeV. *Phys. Rev. C* **2001**, *63*, 064902. [[CrossRef](#)]
49. Bravina, L.V.; Zabrodin, E.E.; Bass, S.A.; Bleicher, M.; Brandstetter, M.; Faessler, A.; Fuchs, C.; Greiner, W.; Soff, S.; Stöcker, H. Microscopic models and effective equation of state in nuclear collisions in the vicinity of $E_{lab} = 30$ AGeV at the GSI Facility for Antiproton and Ion Research (FAIR) and beyond. *Phys. Rev. C* **2008**, *78*, 014907. [[CrossRef](#)]
50. Oliinychenko, D.; Petersen, H. Deviations of the Energy-Momentum Tensor from Equilibrium in the Initial State for Hydrodynamics from Transport Approaches. *Phys. Rev. C* **2016**, *93*, 034905. [[CrossRef](#)]
51. De, S.; De, S.; Chattopadhyay, S. Thermalization of dense hadronic matter in Au + Au collisions at energies available at the Facility for Antiproton and Ion Research. *Phys. Rev. C* **2016**, *94*, 054901. [[CrossRef](#)]
52. Belkacem, M.; Brandstetter, M.; Bass, S.A.; Bleicher, M.; Bravina, L.; Gorenstein, M.I.; Konopka, J.; Neise, L.; Spieles, C.; Soff, S.; et al. Equation of state, spectra and composition of hot and dense infinite hadronic matter in a microscopic transport model. *Phys. Rev. C* **1998**, *58*, 1727–1733. [[CrossRef](#)]
53. Bravina, L.V.; Zabrodin, E.E.; Bass, S.A.; Bleicher, M.; Brandstetter, M.; Soff, S.; Stöcker, H.; Greiner, W. Local equilibrium in heavy ion collisions: Microscopic analysis of a central cell versus infinite matter. *Phys. Rev. C* **2000**, *62*, 064906. [[CrossRef](#)]
54. Bratkovskaya, E.L.; Cassing, W.; Greiner, C.; Effenberger, M.; Mosel, U.; Sibirtsev, A. Aspects of thermal and chemical equilibration of hadronic matter. *Nucl. Phys. A* **2000**, *675*, 661–691. [[CrossRef](#)]